# A Qualitative Study on Optimized MOSFET Doping Profiles

M. Stockinger, R. Strasser, R. Plasun, A. Wild[†], and S. Selberherr

Institute for Microelectronics, TU Vienna
Gusshausstr. 27–29, A-1040 Vienna, Austria
[†]Motorola
Tempe, AZ 85284, USA

Abstract

We present the two-dimensional optimization of the acceptor doping profile of a 0.25 $\mu$m MOSFET which improves the drive current by 48% compared to a uniformly doped device delivering the same drain-source leakage current. Various values for the supply voltage and the allowed leakage current are used to qualitatively investigate their influence on the optimal profile.

## 1. Introduction

High performance ULSI technology requires devices with optimized characteristics. In the past various device structures have been reported for MOSFETs with different aims, e.g. improving short-channel effects, drive current, leakage current, gate delay, etc. Low-power applications became more and more important because of the growing portable electronics market. Supply voltage will continuously be reduced for future device generations in order to reduce the power consumption and to enable single-battery operation. Very low off-state currents are needed to meet the standby power requirements.

Optimizations performed by hand or manually controlled simulations are no longer suitable for complex performance goals. Therefore, a fast self-contained device optimization process is required. Parameters like device structure, supply voltage, or allowed drain-source leakage current have a strong influence on the optimization results. General dependencies on these parameters can be found to give a guideline for the design of optimal doping profiles.

## 2. Two-Dimensional Optimization

We performed an acceptor doping profile optimization of an n-MOSFET with 0.25 $\mu$m gate length, 1 $\mu$m gate width, 5 nm gate-oxide thickness, 83 nm S/D-spacer length, 50 nm S/D-junction depth, $10^{20}$ cm$^{-3}$ S/D surface donor doping, $10^{12}$ cm$^{-3}$ substrate donor doping (Fig. 1), and $10^{17}$ cm$^{-3}$ substrate acceptor doping. The goal is to achieve maximum drive current $I_{on}$ for a supply voltage $V_{dd} = 1.5$ V while at the same time keeping the drain-source leakage current $I_{off}$ below 1 pA. For optimization purposes

we have to combine this constraint with the goal to a global optimization target which reads:

$$\text{target}(I_{on}, I_{off}) = \text{penalty}(I_{off}) - I_{on}, \tag{1}$$

where we make use of a half-parabolic penalty function for $I_{off}$:

$$\text{penalty}(I_{off}) = \begin{cases} 10^{19} A^{-1} \cdot (I_{off} - 1pA)^2 & : \; I_{off} > 1pA \\ 0 & : \; I_{off} <= 1pA. \end{cases} \tag{2}$$

The global optimization target (1) is minimized using a nonlinear optimizer. A discretization of the acceptor-doping region between the source- and drain-wells is performed. Fig. 2 shows the 49 discretization points at the intersections of the drawn mesh. The acceptor doping in the channel region is obtained by superposition of 49 raised-cosine shaped doping fragments in the logarithmic domain. For each optimization step two device simulations (for $I_{on}$ and $I_{off}$) are carried out with MINIMOS-NT [1]. The whole optimization process is controlled by the VISTA framework [2] which allows extensiv parallel execution of system jobs.

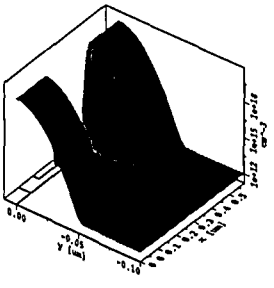

Figure 1: Donor doping.

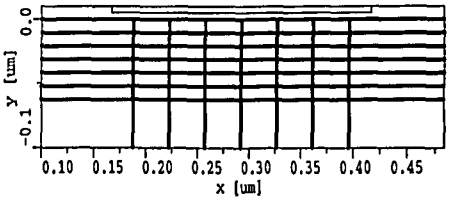


Figure 2: Discretization.

One optimization step is as follows (Fig. 3):

- the optimizer requests an evaluation with a set of doping parameters
- the device description (geometry, doping, and simulation-grid) is produced by an analytical device generator using this parameter set
- the required device simulations are carried out by the simulator
- the global optimization target is calculated and returned to the optimizer

Fig. 4 shows the optimization result. $I_{on}$ was improved by 48% compared to a uniformly doped device with $N_{sub} = 6.25 \cdot 10^{17}$ cm$^{-3}$ delivering the same $I_{off}$.

## 3. Sensitivity Analysis

The obtained doping profile looks complex, but can be simplified. To identify the critical doping parameters a sensitivity analysis is carried out. In the analysis each of the 49 doping parameters is slightly increased by a constant value of 0.0025 in the logarithmic domain, the device description is produced using the changed parameter set, and two device simulations are performed to find $I_{on}$ and $I_{off}$. Then the optimization target is calculated using (1) and its relative deviation from the original target is visualized on the discretization grid of Fig. 2 using the same interpolation method as for the doping (Fig. 5). One important region near the surface at the source side can be identified. The doping parameters outside this region have about one order of magnitude less impact on the device performance, therefore these parameters can be chosen more or less arbitrarily.

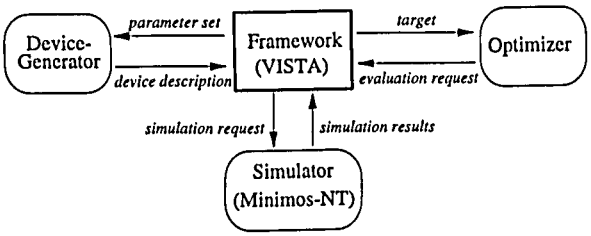


Figure 3: Optimization process.

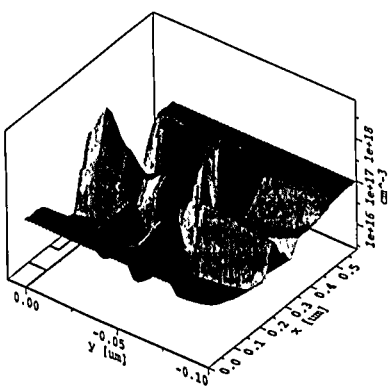

Figure 4: Optimized acceptor doping.

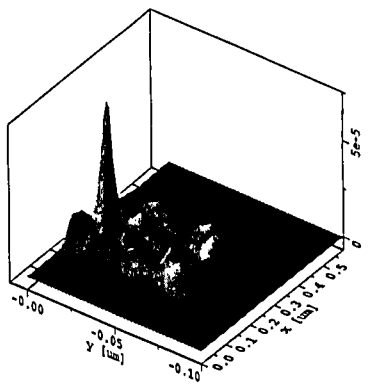

Figure 5: Optimization-target sensitivity.

## 4. Implantation Model

The two-dimensional acceptor doping of Fig. 4 can be substituted by one adjustable Gaussian implantation model without any remarkable performance loss. Further optimization processes were performed using this model. Parameters are substrate doping $N_{sub}$, peak doping $N_{peak}$, lateral and vertical center position $x$ and $y$, implantation length $\Delta x$, and lateral and vertical standard deviations $\sigma_x$ and $\sigma_y$. Results for some representative pairs of $I_{off}$ and $V_{dd}$ are listed in Tab. 1 and shown in Fig. 6 for comparison. Amazingly enough, the doping profile comes close to the FIBMOS structure presented in [3].

Table 1: Optimization results for the implantation model.

| $V_{dd}$ | (V) | 0.5 | 1 | 1.5 | 1.5 | 1.5 |
|---|---|---|---|---|---|---|
| $I_{off}$ | (pA) | ~1 | ~1 | ~1 | ~10 | ~100 |
| $I_{on}$ | ($\mu$A) | 4.615 | 152.3 | 361.4 | 400.3 | 434.5 |
| $N_{sub}$ | ($cm^{-3}$) | $1.14 \cdot 10^{16}$ | $3.05 \cdot 10^{16}$ | $2.14 \cdot 10^{16}$ | $1.51 \cdot 10^{16}$ | $6.46 \cdot 10^{15}$ |
| $N_{peak}$ | ($cm^{-3}$) | $8.64 \cdot 10^{17}$ | $1.67 \cdot 10^{18}$ | $1.35 \cdot 10^{18}$ | $1.32 \cdot 10^{18}$ | $1.10 \cdot 10^{18}$ |
| $x$ | ($\mu$m) | 0.285 | 0.2504 | 0.2398 | 0.2356 | 0.2333 |
| $y$ | ($\mu$m) | 0.0108 | 0.01561 | 0.0135 | 0.0202 | 0.0226 |
| $\Delta x$ | ($\mu$m) | 0.0698 | 0.0197 | 0.00266 | 0.00016 | 0.00707 |
| $\sigma_x$ | ($\mu$m) | 0.03516 | 0.01362 | 0.01914 | 0.01521 | 0.01 |
| $\sigma_y$ | ($\mu$m) | 0.01723 | 0.01003 | 0.02034 | 0.02327 | 0.03962 |
| $\Delta x + 2\sigma_x$ | ($\mu$m) | 0.14012 | 0.04694 | 0.04094 | 0.03058 | 0.02707 |

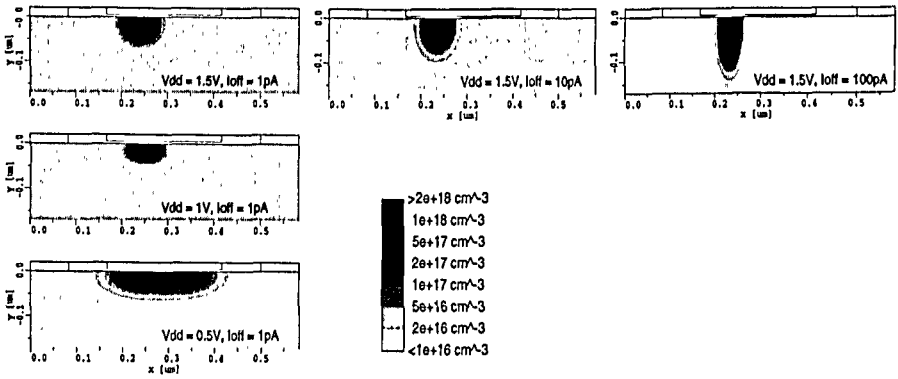


Figure 6: Optimized acceptor doping for various $I_{off}$ (horiz.) and $V_{dd}$ (vert.) using a Gaussian implantation model.

## 5. Conclusion

Results from doping-profile optimizations using a Gaussian implantation model showed that for lower $V_{dd}$ the doping peak extends towards the drain side. The performance improvements can be addressed to the exploitation of the different current-voltage relationships for weak and strong inversion. For small $V_{dd}$ values a symmetric doping is expected (see Fig. 6, $V_{dd} = 0.5$ V) because the device will not reach the strong inversion region during operation. For a higher allowed $I_{off}$, $N_{sub}$ and $N_{peak}$ decrease because a higher threshold voltage can be accepted. The overall lateral peak length, approximated by $\Delta x + 2\sigma_x$ decreases as the device is operated deeper in the strong inversion regime.

## Acknowledgment

This work is supported by the "Christian Doppler Forschungsgesellschaft", Vienna, Austria.

## References

[1] T. Simlinger, H. Brech, T. Grave, and S. Selberherr, "Simulation of Submicron Double-Heterojunction High Electron Mobility Transistors with MINIMOS-NT," *IEEE Trans.Electron Devices*, vol. 44, no. 5, pp. 700–707, 1997.

[2] S. Halama, F. Fasching, C. Fischer, H. Kosina, E. Leitner, C. Pichler, H. Pimingstorfer, H. Puchner, G. Rieger, G. Schrom, T. Simlinger, M. Stiftinger, H. Stippel, E. Strasser, W. Tuppa, K. Wimmer, and S. Selberherr, "The Viennese Integrated System for Technology CAD Applications," in *Technology CAD Systems* (F. Fasching, S. Halama, and S. Selberherr, eds.), (Wien), pp. 197–236, Springer, 1993.

[3] C.-C. Shen, J. Murguia, N. Goldsman, M. Peckerar, J. Melngailis, and D. Antoniadis, "Use of Focused-Ion-Beam and Modeling to Optimize Submicron MOSFET Characteristics," *IEEE Trans.Electron Devices*, vol. 45, no. 2, pp. 453–459, 1998.